Electronic Supplementary Material (ESI) for Nanoscale.

Constructing imine groups on the surface of Cu_1/Pd(111) as a novel strategy for CO_2 hydrogenation to methanol

Sanmei Wang,[a,b] Qi Li,[a] Yue Xin,[a] Sunpei Hu,[b] Xiaoxi Guo,[a] Yong Zhang,[c] Ling Zhang,[d] Bingang Chen,*[d] Wenhua Zhang,*[b] Liangbing Wang*[a]

[a] *State Key Laboratory for Powder Metallurgy, School of Materials Science and Engineering, Central South University, Changsha, Hunan 410083*

[b] *Hefei National Laboratory for Physical Sciences at the Microscale and Synergetic Innovation Centre of Quantum Information & Quantum Physics, University of Science and Technology of China, Hefei, Anhui 230026*

[c] *Qinghai Oilfield New Energy Division, Dunhuang, Gansu, 736202*

[d] *Ningbo Fengcheng Advanced Energy Materials Research Institute Co., Ltd., Fenghua District, Ningbo, Zhejiang, 315500*

The calculation details for the catalytic activity of Cu(111), Pd_3Cu_6, Pd_6Cu_3, Pd-ML, and Pd(111) for CO_2 hydrogenation to CH_3OH

The structures of the Cu(111), Pd_3Cu_6, Pd_6Cu_3, and Pd-ML in Fig. 1a were obtained from ref.32. The size for the Cu(111), Pd_3Cu_6, Pd_6Cu_3, and Pd-ML structure were four-layer slabs with (3×3) unit cells (Fig. S1†). Ref. 32 showed that the rate-determining step for CO_2 hydrogenation to CH_3OH over Cu(111), Pd_3Cu_6, Pd_6Cu_3 were the hydrogenation of CO_2 to COOH. For Pd-ML, the the rate-determining step was the O-O bond breaking of the COOH intermediates. To increase the comparability and reduce the computational cost, we recalculated the rate-determining step energy barrier using the parameters of the computational method. Thus, all structures in Fig. 1a were calculated using the same method. The free energy profiles for CO_2 hydrogenation to CH_3OH over Pd(111) was shown in Fig. S2†.

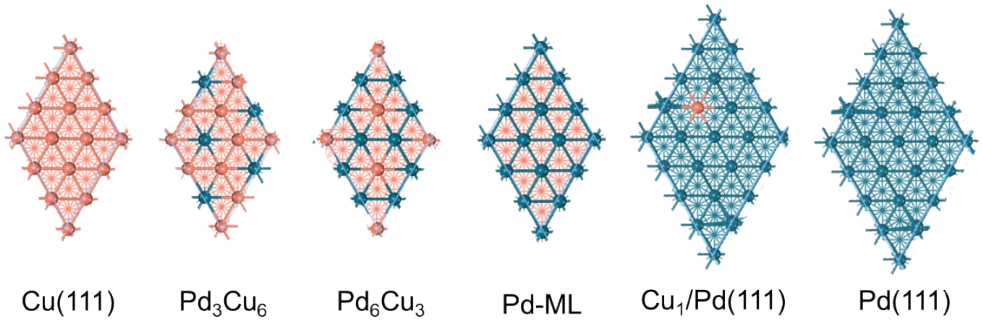

Fig. S1 The various Pd-Cu structures. The cyan and yellow spheres represented Pd and Cu atoms, respectively.

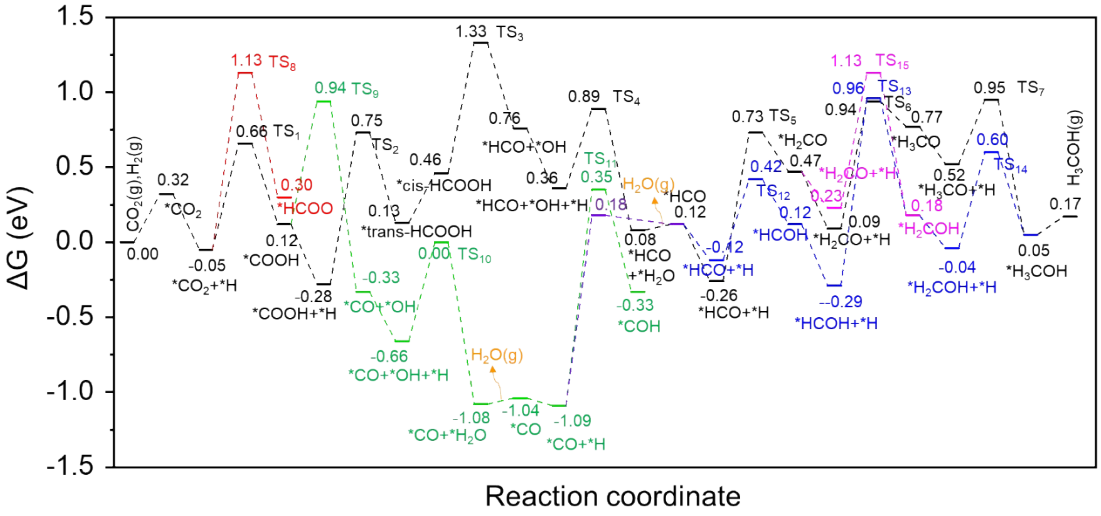

Fig. S2 The free energy profiles for CO_2 hydrogenation to CH_3OH over Pd(111). The black route was the most possible reaction pathway for CO_2 hydrogenation to CH_3OH over Pd(111). TS represented the transition state.

The possible adsorption configuration for CO_2 on C_3H_4O@NH_2-Cu_1/Pd(111)

We established a large number of structures to detect whether CO_2 tended to be adsorbed via the interaction between the C of CO_2 and the N of imine groups. The calculation results indicated that CO_2 was difficult to interact with amine groups on NH_2-Cu_1/Pd(111), C_2H_4O@NH_2-Cu_1/Pd(111), and C_3H_6O@NH_2-Cu_1/Pd(111) due to steric hindrances. Nevertheless, for C_3H_4O@NH_2-Cu_1/Pd(111), CO_2 was able to chemically adsorb on amines by its C atoms bonded to N of amine groups (Fig.S3a†). The adsorption energy of CO_2 in this configuration was -0.22 eV, which was close to that of CO_2 completely adsorbed on Pd atoms (-0.20 eV) (Fig.S3b†). In addition, the adsorption configurations where C and O of CO_2 were bonded to N of amine groups and Pd atoms, respectively, were also considered. Fig.S3c† illustrated that the adsorption energy of CO_2 in this configuration was -0.27 eV, which was still close to that of CO_2 completely adsorbed on Pd atoms (-0.20 eV). The results indicated that the N atoms of imines and the Pd atoms next to the imines were possible adsorption sites for CO_2. Nevertheless, CO_2 adsorbed entirely on Pd was more conducive to its binding with H to generate CH_3OH than CO_2 adsorbed on imines. Thus, the most optimal adsorption configuration for CO_2 hydrogenation to CH_3OH on C_3H_4O@NH_2-Cu_1/Pd(111) was CO_2 adsorbed entirely on Pd atoms.

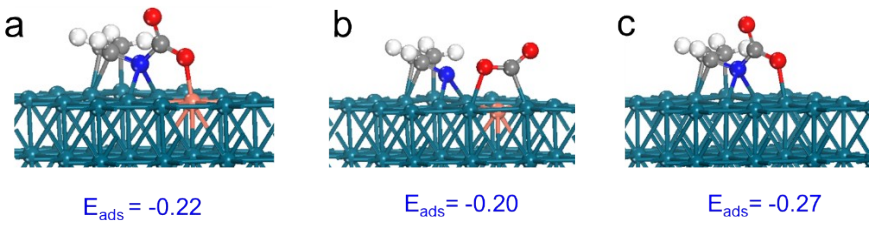

Fig. S3 The possible adsorption configuration of CO_2 on C_3H_4O@NH_2-Cu_1/Pd(111). The cyan, grey, white, blue, red, and yellow spheres represented Pd, C, H, N, O, and Cu atoms,

respectively.

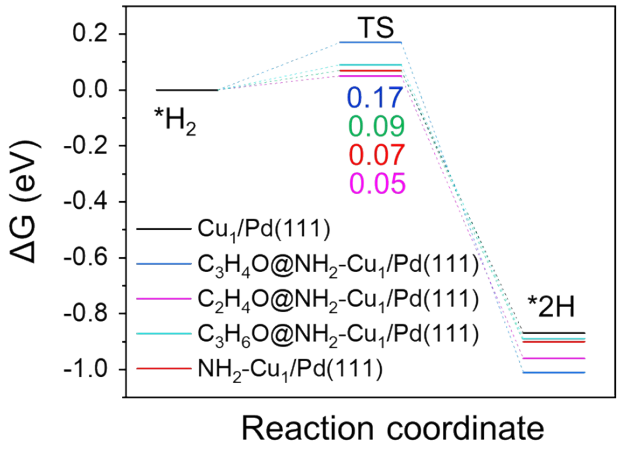

Fig. S4 The dissociation of H_2 on various structures. TS represented the transition state.

Table S1 The free energy barriers (eV) of elementary steps for CO_2 hydrogenation to CH_3OH over Cu_1/Pd(111), NH_2-Cu_1/Pd(111), C_2H_4O@NH_2-Cu_1/Pd(111), C_3H_4O@NH_2-Cu_1/Pd(111), and C_3H_6O@NH_2-Cu_1/Pd(111).

No.	Reactions	Cu_1/ Pd(111)	NH_2-Cu_1/ Pd(111)	C_2H_4O@ NH_2-Cu_1/ Pd(111)	C_3H_4O @NH_2-Cu_1/ Pd(111)	C_3H_6O @NH_2-Cu_1/ Pd(111)
R_1	CO_2*+*H→*COOH	0.63	0.59	0.59	0.56	0.56
R_2	CO_2*+*H→*HCOO	0.76	0.74	0.76	0.90	0.80
R_3	*COOH→*CO+*OH	1.42	1.47	0.72	0.80	0.80
R_4	*CO+*OH+*H→*CO+ *H_2O	0.60	0.64	0.53	0.95	0.61
R_5	*CO+*H→*COH	1.86	1.43	1.52	1.41	1.40
R_6	*CO+*H→*HCO	1.95	1.15	1.20	1.35	1.24
R_7	*COOH+*H→*trans-HCOOH	1.00	0.88	0.78	0.62	0.86
R_8	*trans-HCOOH→*cis-HCOOH	0.81	0.55	0.59	0.60	0.74
R_9	*cis-HCOOH→*HCO+*OH	0.62	0.47	0.43	0.62	0.74
R_{10}	*HCO+*OH+*H→*HCO+*H_2O	0.74	0.80	0.47	0.48	0.69
R_{11}	*HCO+*H→*HCOH	0.60	0.57	0.54	0.66	0.78
R_{12}	*HCOH+*H→*H_2COH	1.48	0.72	1.03	0.65	0.82
R_{13}	*H_2COH+*H→*H_3COH	0.70	0.74	0.62	0.61	0.71
R_{14}	*HCO+*H→*H_2CO	0.90	1.01	0.79	0.83	0.68
R_{15}	*H_2CO+*H→*H_2COH	1.32	0.81	0.89	0.45	0.84
R_{16}	*H_2CO+*H→*H_3CO	0.72	0.75	0.78	0.82	0.62
R_{17}	*H_3CO+*H→*H_3COH	0.29	0.30	0.55	0.36	0.26

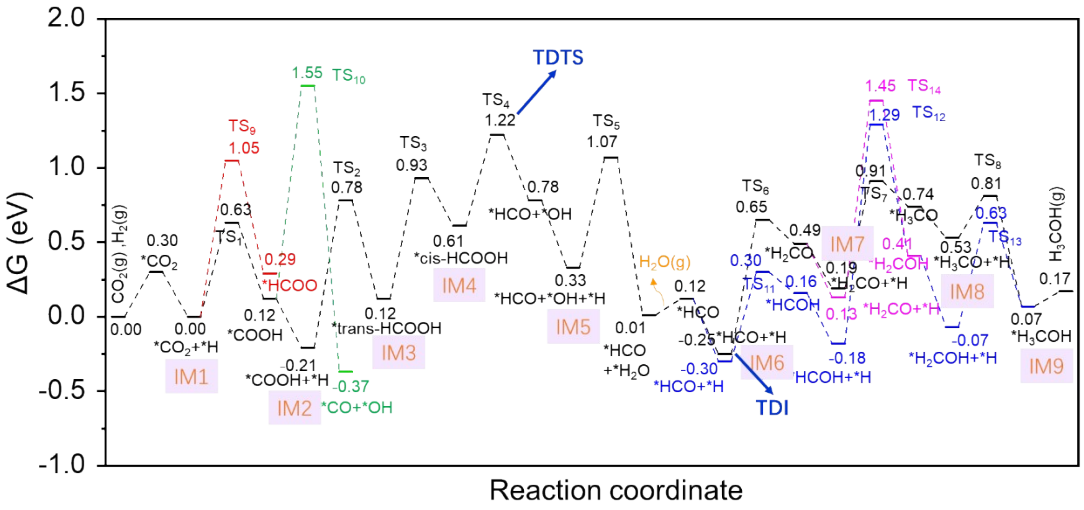

Fig. S5 The free energy profiles for CO_2 hydrogenation to CH_3OH over Cu_1/Pd(111). The black route was the most possible reaction pathway for CO_2 hydrogenation to CH_3OH over Cu_1/Pd(111). TS represented the transition state. IM represented the intermediates used to calculate the X_{TOF}.

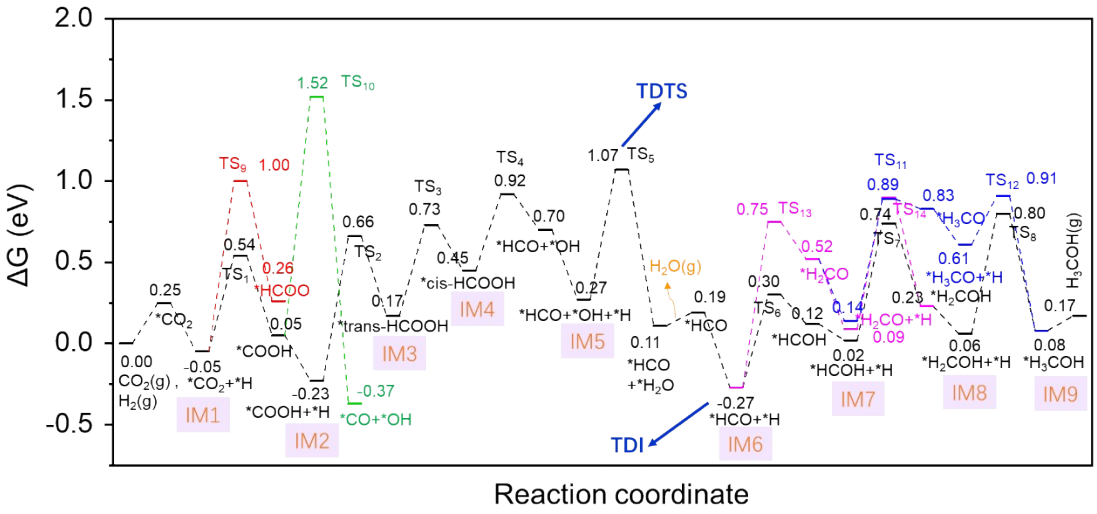

Fig. S6 The free energy profiles for CO_2 hydrogenation to CH_3OH over NH_2-Cu_1/Pd(111). The black route was the most possible reaction pathway for CO_2 hydrogenation to CH_3OH over NH_2-Cu_1/Pd(111). TS represented the transition state. IM represented the intermediates used to calculate the X_{TOF}.

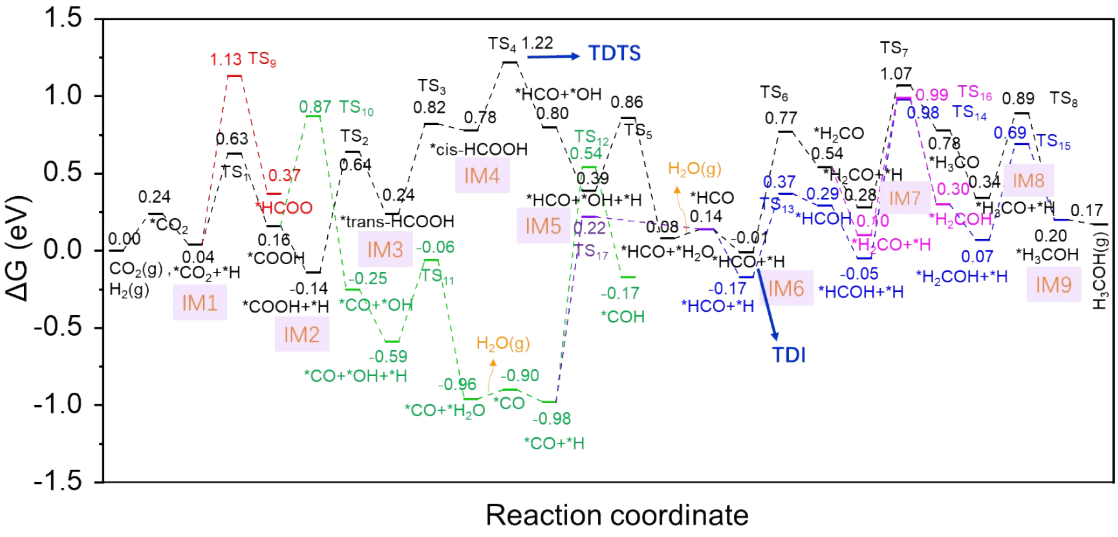

Fig. S7 The free energy profiles for CO_2 hydrogenation to CH_3OH over C_2H_4O@NH_2-Cu_1/Pd(111). The black route was the most possible reaction pathway for CO_2 hydrogenation to CH_3OH over C_2H_4O@NH_2-Cu_1/Pd(111). TS represented the transition state. IM represented the intermediates used to calculate the X_{TOF}.

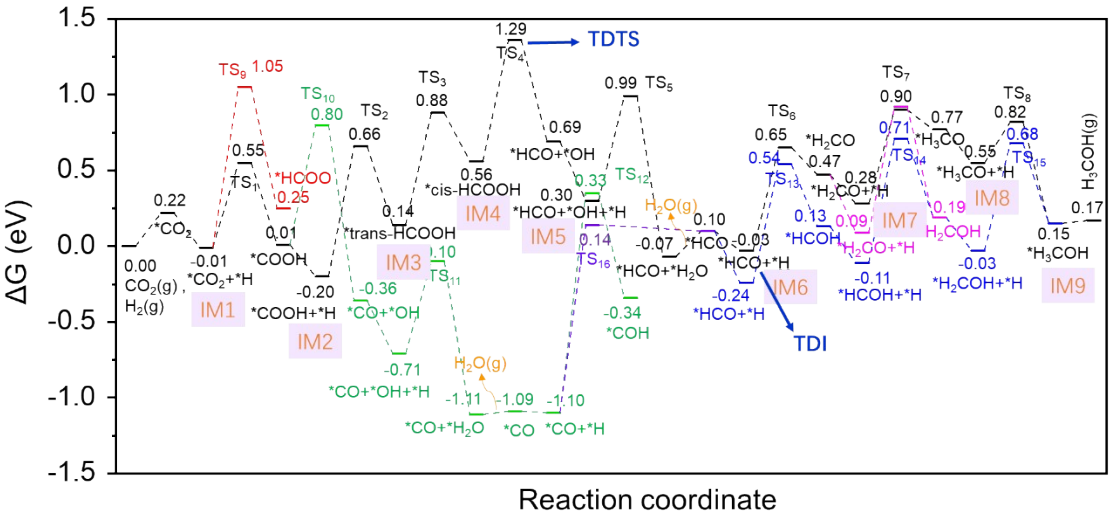

Fig. S8 The energy profiles for CO_2 hydrogenation to CH_3OH over C_3H_6O@NH_2-Cu_1/Pd(111). The black route was the most possible reaction pathway for CO_2 hydrogenation to CH_3OH over C_3H_6O@NH_2-Cu_1/Pd(111). TS represented the transition state. IM represented the intermediates used to calculate the X_{TOF}.

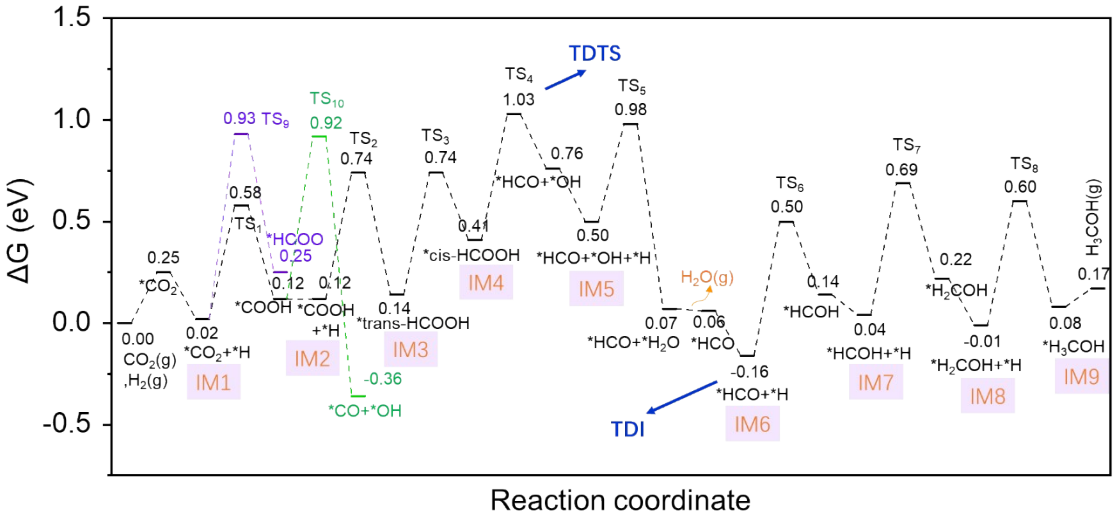

Fig. S9 The free energy profiles for CO_2 hydrogenation to CH_3OH over C_3H_4O@NH_2-Cu_1/Pd(111). IM represented the intermediates used to calculate the X_{TOF}.

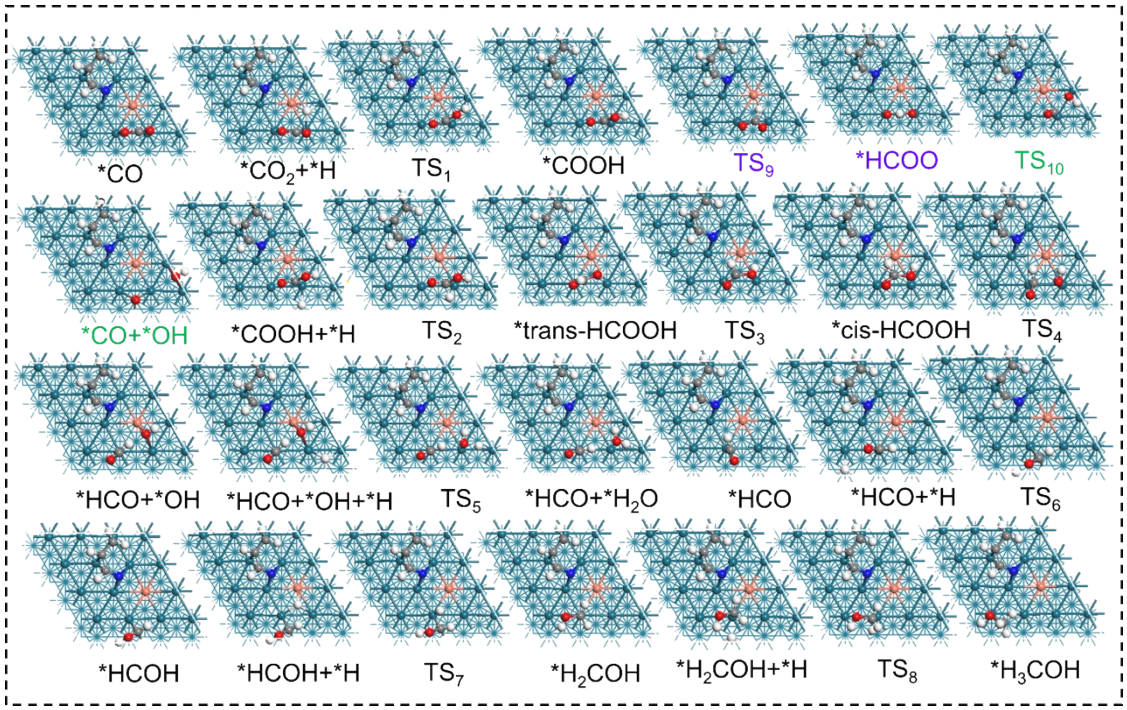

Fig. S10 The structures of intermediates in the hydrogenation of CO_2 to CH_3OH on C_3H_4O@NH_2-Cu_1/Pd(111). The cyan, grey, white, blue, red, and yellow spheres represented Pd, C, H, N, O, and Cu atoms, respectively.

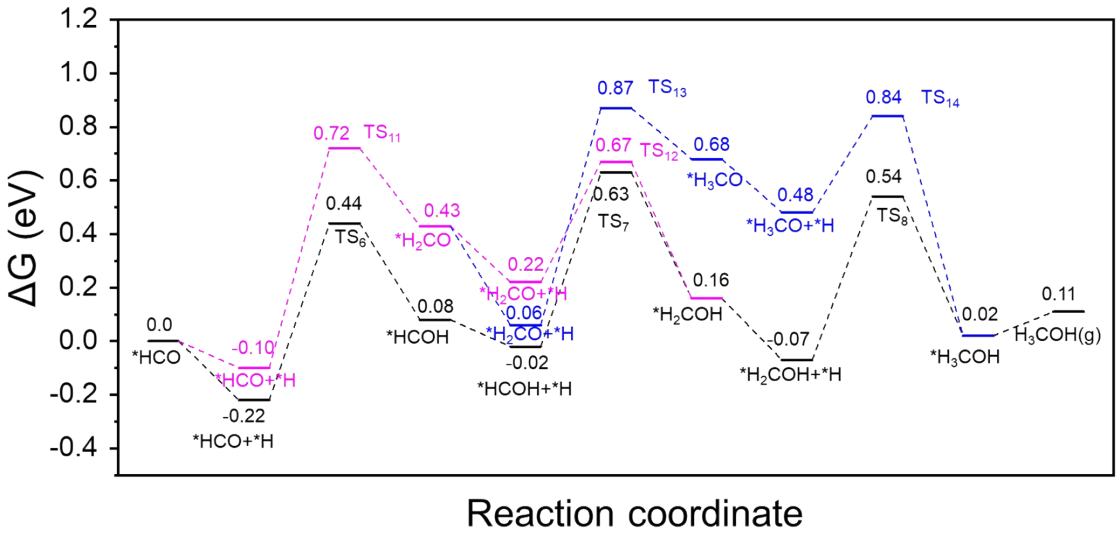

Fig. S11 The possible reaction paths from HCO intermediates hydrogenation to CH_3OH over C_3H_4O@NH_2-Cu_1/Pd(111).

Energetic span model

The energetic span model proposed by Kozuch[S1-S2] were used to estimate turnover frequency (TOF). Energetic span model theory suggested that the energy span (δE) determined the reaction rate in the catalytic cycle of multi-element steps, rather than the step with the highest activation energy. δE can be obtained by TOF-determining intermediate (TDI) and TOF-determining transition state (TDTS). The Gibbs free energy difference of the total reaction was named as ΔGr. When ΔGr < 0, the approximate relation between TOF and energy span δE can be simplified to

$$TOF = \frac{k_B T}{h} exp(-\frac{\delta E}{RT}) \quad (1)$$

$$\delta E = \begin{cases} T_{TDTS} - I_{TDI} & if\ TDTS\ appears\ after\ TDI \\ T_{TDTS} - I_{TDI} + \Delta G_r & if\ TDTS\ appears\ before\ TDI \end{cases} \quad (2)$$

Where K_B is Boltzmann constant, T is temperature, and R is the ideal gas constant. To locate the determining states, we can calculate the degree of TOF control for transition states and intermediates ($X_{TOF,T}$ and $X_{TOF,I}$). The states with the highest X_{TOF} corresponded to the TDTS and TDI.[S3]

$$X_{TOF,T_i} = \frac{\sum_j exp[(T_i - I_j - \Delta G_{ij})/RT]}{\sum_i \sum_j exp[(T_i - I_j - \Delta G_{ij})/RT]} \quad (3)$$

$$X_{TOF,T_j} = \frac{\sum_i exp[(T_i - I_j - \Delta G_{ij})/RT]}{\sum_i \sum_j exp[(T_i - I_j - \Delta G_{ij})/RT]} \quad (4)$$

$$\Delta G_{ij} = \begin{cases} \Delta G_r, & i > j, \\ 0, & i \le j. \end{cases}$$

Where I_i and T_i symbolized the standard-state Gibbs energies of the ith intermediate or transition state. The X_{TOF} of the ith intermediate and transition states on Cu_1/Pd(111), NH_2-Cu_1/Pd(111), C_2H_4O@NH_2-Cu_1/Pd(111), C_3H_4O@NH_2-Cu_1/Pd(111) and C_3H_6O@NH_2-Cu_1/Pd(111) were displayed in Table S2, Table S3, Table S4, Table S5, and Table S6,

respectively. We only considered the X_{TOF} of intermediates and transition states in the optimal pathway. X_{TOF} showed that for NH_2-Cu_1/Pd(111), the TDI and TDTS were IM6 and TS_5, respectively. For Cu_1/Pd(111), C_2H_4O@NH_2-Cu_1/Pd(111), C_3H_4O@NH_2-Cu_1/Pd(111), C_3H_6O@NH_2-Cu_1/Pd(111), the TDI and TDTS were IM6 and TS_4, respectively. It was noted that the X_{TOF} of IM2 and IM6 in C_3H_6O@NH_2-Cu_1/Pd(111) were the same. COOH intermediate hydrogenated to trans-HCOOH intermediate was endothermic 0.34 eV, while HCO intermediate hydrogenated to H_2CO intermediate was endothermic 0.50 eV. The result indicated that IM6 had a more significant effect on the whole reaction than IM2. Thus, we chose IM6 as the TDI for CO_2 hydrogenation to CH_3OH on C_3H_6O@NH_2-Cu_1/Pd(111). After TDI and TDTS were determined, δE can be calculated according to equation (2). The δE for Cu_1/Pd(111), NH_2-Cu_1/Pd(111), C_2H_4O@NH_2-Cu_1/Pd(111), C_3H_4O@NH_2-Cu_1/Pd(111), and C_3H_6O@NH_2-Cu_1/Pd(111) were 1.47, 1.34, 1.23, 1.19, and 1.32 eV, respectively.

Table S2 The X_{TOF} of intermediates and transition states on Cu_1/Pd(111).

	IM1	IM2	IM3	IM4	IM5	IM6	IM7	IM8	IM9	X_{TOF}, T_i
T_1	3.34E+10	1.07E+14	3.30E+08	2.16E+00	1.03E+05	5.00E+14	2.24E+07	4.68E+01	2.26E+09	1.69E-10
T_2	1.55E+10	3.44E+16	1.06E+11	6.91E+02	3.29E+07	1.60E+17	7.16E+09	1.50E+04	7.24E+11	5.41E-08
T_3	4.95E+12	1.59E+16	3.39E+13	2.21E+05	1.05E+10	5.13E+19	2.29E+12	4.80E+06	2.32E+14	1.43E-05
T_4	3.46E+17	1.11E+21	3.42E+15	1.55E+10	7.35E+14	3.58E+24	1.60E+17	3.35E+11	1.62E+19	9.97E-01
T_5	1.08E+15	3.48E+18	1.07E+13	6.98E+04	2.29E+12	1.12E+22	5.00E+14	1.05E+09	5.05E+16	3.11E-03
T_6	1.04E+08	3.35E+11	1.03E+06	6.74E-03	3.20E+02	1.08E+15	4.83E+07	1.01E+02	4.88E+09	3.00E-10
T_7	2.29E+12	7.39E+15	2.27E+10	1.48E+02	7.05E+06	3.44E+16	1.06E+12	2.23E+06	1.07E+14	1.17E-08
T_8	4.90E+10	1.58E+14	4.85E+08	3.17E+00	1.51E+05	7.35E+14	3.29E+07	4.75E+04	2.29E+12	2.49E-10
X_{TOF}, I_j	9.65E-08	3.11E-04	9.64E-10	4.30E-15	2.05E-10	1.00E+00	4.47E-08	9.35E-14	4.52E-06	

Table S3 The X_{TOF} of intermediates and transition states on NH_2-Cu_1/Pd(111).

	IM1	IM2	IM3	IM4	IM5	IM6	IM7	IM8	IM9	X_{TOF}, T_i
T_1	7.16E+09	7.27E+12	1.51E+06	3.19E+01	3.24E+04	3.39E+13	4.85E+08	1.04E+08	4.83E+07	1.70E-09
T_2	1.05E+09	7.35E+14	1.53E+08	3.22E+03	3.27E+06	3.42E+15	4.90E+10	1.05E+10	4.88E+09	1.72E-07
T_3	1.55E+10	1.57E+13	2.26E+09	4.75E+04	4.83E+07	5.05E+16	7.24E+11	1.55E+11	7.20E+10	2.09E-06
T_4	2.31E+13	2.34E+16	4.88E+09	7.09E+07	7.20E+10	7.54E+19	1.08E+15	2.32E+14	1.07E+14	3.11E-03
T_5	7.39E+15	7.50E+18	1.56E+12	3.29E+07	2.31E+13	2.41E+22	3.46E+17	7.42E+16	3.44E+16	9.97E-01
T_6	1.02E+03	1.03E+06	2.15E-01	4.52E-06	4.59E-03	3.32E+09	4.75E+04	1.02E+04	4.73E+03	1.37E-13
T_7	2.27E+10	2.31E+13	4.80E+06	1.01E+02	1.03E+05	1.07E+14	1.06E+12	2.28E+11	1.06E+11	5.44E-09
T_8	2.28E+11	2.32E+14	4.83E+07	1.02E+03	1.03E+06	1.08E+15	1.55E+10	2.29E+12	1.06E+12	5.43E-08
X_{TOF}, I_j	3.06E-07	3.11E-04	6.48E-11	4.28E-15	9.55E-10	1.00E+00	1.43E-05	3.07E-06	1.42E-06	

Table S4 The X_{TOF} of intermediates and transition states on C_2H_4O@NH_2-Cu_1/Pd(111).

	IM1	IM2	IM3	IM4	IM5	IM6	IM7	IM8	IM9	X_{TOF}, T_i
T_1	7.16E+09	7.27E+12	3.27E+06	3.12E-03	1.02E+04	4.90E+10	7.02E+05	6.98E+04	1.52E+07	1.72E-08
T_2	1.52E+07	1.07E+13	4.80E+06	4.59E-03	1.50E+04	7.20E+10	1.03E+06	1.03E+05	2.24E+07	2.52E-08
T_3	1.55E+10	1.57E+13	4.88E+09	4.66E+00	1.52E+07	7.31E+13	1.05E+09	1.04E+08	2.27E+10	2.08E-07
T_4	7.42E+16	7.54E+19	3.39E+13	2.24E+07	7.31E+13	3.51E+20	5.03E+15	5.00E+14	1.09E+17	9.99E-01
T_5	7.20E+10	7.31E+13	3.29E+07	3.14E-02	7.09E+07	3.41E+14	4.88E+09	4.85E+08	1.06E+11	9.69E-07
T_6	2.26E+09	2.29E+12	1.03E+06	9.85E-04	3.22E+03	1.07E+13	1.53E+08	1.52E+07	3.32E+09	3.04E-08
T_7	2.32E+14	2.35E+17	1.06E+11	1.01E+02	3.30E+08	1.59E+15	1.57E+13	1.56E+12	3.41E+14	5.56E-04
T_8	2.28E+11	2.32E+14	1.04E+08	9.95E-02	3.25E+05	1.56E+12	2.24E+07	1.54E+09	3.35E+11	5.48E-07
X_{TOF}, I_j	1.74E-04	1.77E-01	7.96E-08	5.24E-14	1.71E-07	8.22E-01	1.18E-05	1.18E-06	2.56E-04	

Table S5 The X_{TOF} of intermediates and transition states on C_3H_4O@NH_2-Cu_1/Pd(111).

	IM1	IM2	IM3	IM4	IM5	IM6	IM7	IM8	IM9	X_{TOF}, T_i
T_1	2.26E+09	4.83E+07	2.24E+07	6.91E+02	2.17E+01	2.29E+12	1.05E+09	7.16E+09	2.25E+08	2.66E-08
T_2	1.54E+09	2.27E+10	1.05E+10	3.25E+05	1.02E+04	1.08E+15	4.93E+11	3.37E+12	1.06E+11	1.25E-05
T_3	1.54E+09	3.29E+07	1.05E+10	3.25E+05	1.02E+04	1.08E+15	4.93E+11	3.37E+12	1.06E+11	1.25E-05
T_4	1.07E+14	2.29E+12	1.06E+12	2.27E+10	7.13E+08	7.54E+19	3.44E+16	2.35E+17	7.39E+15	8.72E-01
T_5	1.57E+13	3.35E+11	1.55E+11	4.80E+06	1.04E+08	1.10E+19	5.03E+15	3.44E+16	1.08E+15	1.28E-01
T_6	1.51E+05	3.22E+03	1.49E+03	4.61E-02	1.45E-03	1.06E+11	4.83E+07	3.30E+08	1.04E+07	1.22E-09
T_7	2.25E+08	4.80E+06	2.23E+06	6.88E+01	2.16E+00	2.28E+11	7.20E+10	4.93E+11	1.55E+10	9.32E-09
T_8	7.05E+06	1.51E+05	6.98E+04	2.16E+00	6.77E-02	7.16E+09	3.27E+06	1.55E+10	4.85E+08	2.67E-10
X_{TOF}, I_j	1.42E-06	3.06E-08	1.43E-08	2.62E-10	9.42E-12	9.96E-01	4.55E-04	3.11E-03	9.76E-05	

Table S6 The X_{TOF} of intermediates and transition states on C_3H_6O@NH_2-Cu_1/Pd(111).

	IM1	IM2	IM3	IM4	IM5	IM6	IM7	IM8	IM9	X_{TOF}, T_i
T_1	2.26E+09	3.37E+12	7.05E+06	6.81E-01	1.50E+04	4.88E+09	3.24E+04	1.00E+00	4.80E+06	1.51E-10
T_2	2.25E+08	2.32E+14	4.85E+08	4.68E+01	1.03E+06	3.35E+11	2.23E+06	6.88E+01	3.30E+08	1.04E-08
T_3	1.06E+12	1.59E+15	2.29E+12	2.21E+05	4.88E+09	1.59E+15	1.05E+10	3.25E+05	1.56E+12	1.42E-07
T_4	7.50E+18	1.12E+22	2.34E+16	1.56E+12	3.44E+16	1.12E+22	7.42E+16	2.29E+12	1.10E+19	1.00E+00
T_5	7.31E+13	1.09E+17	2.28E+11	2.20E+04	3.35E+11	1.09E+17	7.24E+11	2.24E+07	1.07E+14	9.75E-06
T_6	1.53E+08	2.28E+11	4.78E+05	4.61E-02	1.02E+03	2.28E+11	1.51E+06	4.68E+01	2.25E+08	2.04E-11
T_7	2.29E+12	3.42E+15	7.16E+09	6.91E+02	1.52E+07	4.95E+12	2.27E+10	7.02E+05	3.37E+12	1.53E-07
T_8	1.06E+11	1.58E+14	3.30E+08	3.19E+01	7.02E+05	2.28E+11	1.51E+06	3.24E+04	1.55E+11	7.07E-09
X_{TOF}, I_j	3.35E-04	5.00E-01	1.05E-06	6.97E-11	1.54E-06	5.00E-01	3.31E-06	1.02E-10	4.92E-04	

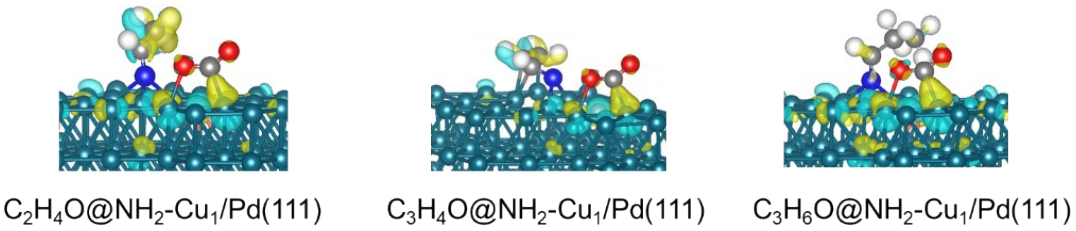

Fig. S12 The charge density difference for CO_2 adsorbed on $C_2H_4O@NH_2$-Cu_1/Pd(111), $C_3H_4O@NH_2$-Cu_1/Pd(111), and $C_3H_6O@NH_2$-Cu_1/Pd(111). The isosurface value was set to 0.02 e/Å^3. The cyan, grey, white, blue, red, and yellow spheres represented Pd, C, H, N, O, and Cu atoms, respectively.

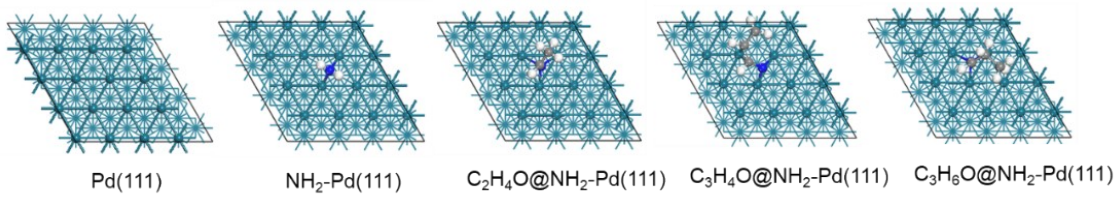

Fig. S13 After the Cu atoms in Cu_1/Pd(111), NH_2-Cu_1/Pd(111), C_2H_4O@NH_2-Cu_1/Pd(111), C_3H_4O@NH_2-Cu_1/Pd(111) and C_3H_6O@NH_2-Cu_1/Pd(111) were replaced by Pd atoms, these structures are named as Pd(111), NH_2-Pd(111), C_2H_4O@NH_2-Pd(111), C_3H_4O@NH_2-Pd(111) and C_3H_6O@NH_2-Pd(111), repectively.

Table S7 The adsorption energy (eV) of CO_2, groups, and H atoms on various structures. ICOHP represented integrated crystal orbital Hamilton population.

structures	$E_{ads}(CO_2)$	E_{ads}(groups)	$E_{ads}(H)$	ICOHP
Pd(111)	-0.11	—	-0.70	-2.28
Cu_1/Pd(111)	-0.12	—	-0.62	-2.33
NH_2-Pd(111)	-0.16	-2.67	-0.67	-2.40
NH_2-Cu_1/Pd(111)	-0.19	-2.71	-0.61	-2.46
C_2H_4O@NH_2-Pd(111)	-0.20	-2.64	-0.68	-2.44
C_2H_4O@NH_2-Cu_1/Pd(111)	-0.22	-2.64	-0.62	-2.47
C_3H_4O@NH_2-Pd(111)	-0.17	-3.34	-0.67	-2.47
C_3H_4O@NH_2-Cu_1/Pd(111)	-0.20	-3.36	-0.62	-2.51
C_3H_6O@NH_2-Pd(111)	-0.21	-2.75	-0.67	-2.45
C_3H_6O@NH_2-Cu_1/Pd(111)	-0.24	-2.76	-0.62	-2.49

Table S8 The energy barriers of the rate-determining steps for CO_2 hydrogenation to CH_3OH over various catalysts.

Catalysts	Energy barriers (eV)	Free energy barriers (eV)	TOF(S^{-1})	References
C_3H_4O@NH_2-Cu_1/Pd(111)	0.72	0.66	-8.24E^{-08}	*This work*
ZnO/Cu(111)	0.90	—	—	S4
Ga_3Ni_5(111)	0.85	—	—	S5
$Zr_3O_6H_6$/Cu(111)	1.36	—	—	S6
SiC quantum dots	1.36	—	—	S7
In_2O_3(110)	1.14	—	—	S8
Cu@Pd core–shell	1.17	—	—	S9
$PdCu_3$(111)	1.40	—	—	S10
Pd_3Cu_6	1.43	—	—	S11
Pd-ML	1.41	—	—	S11

Table S9 The number electrons gained by groups before (e_{before}) and after CO_2 adsorption (e_{after}). The difference in the number of electrons (Δe) obtained by groups before and after CO_2 adsorption.

Structures	e_{before}	e_{after}	Δe
NH_2-Cu_1/Pd(111)	0.16	0.13	0.03
C_2H_4O@NH_2-Cu_1/Pd(111)	0.22	0.18	0.04
C_3H_4O@NH_2-Cu_1/Pd(111)	0.29	0.24	0.05
C_3H_6O@NH_2-Cu_1/Pd(111)	0.23	0.20	0.03

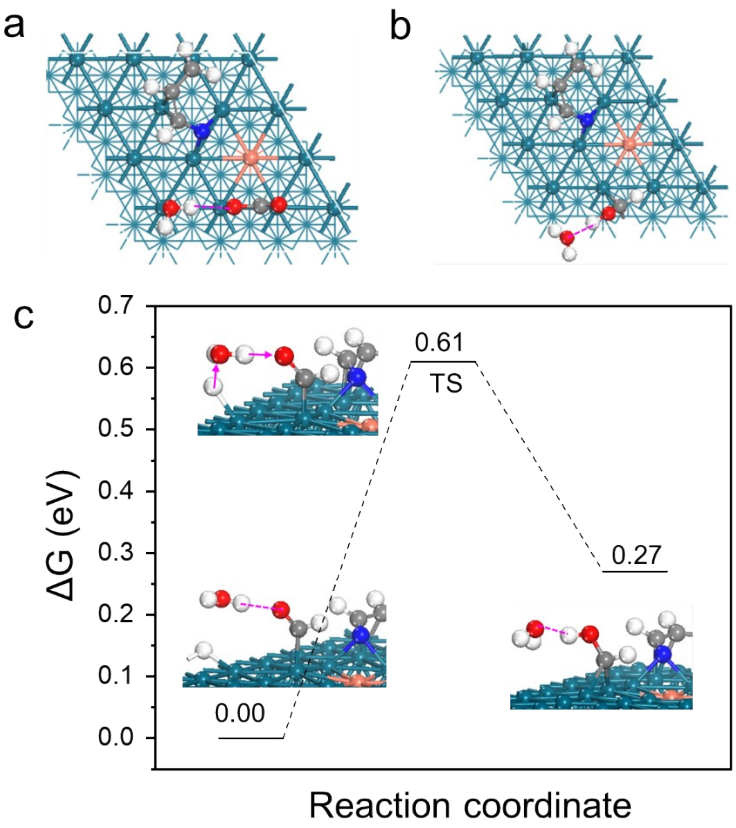

Fig. S14 The effect of H_2O on (a) CO_2 adsorption energy, (b) HCOH intermediates, (c) the energy barriers of rate-determining step on C_3H_4O@NH_2-Cu_1/Pd(111). The red dotted lines represented hydrogen bonds.

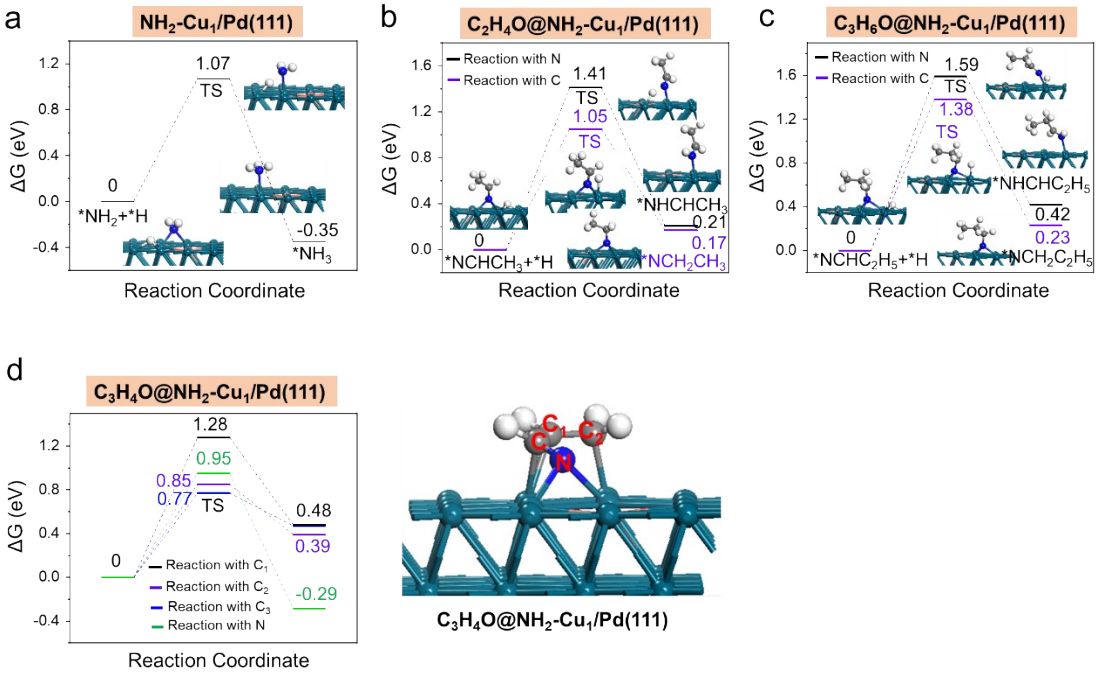

Fig. S15 The free energy profiles for H reactions with groups. (a) The reaction of H with -NH_2 generating -NH_3 over NH_2-Cu_1/Pd(111). (b) The reaction of H with the N atoms (black routes) and C atoms (purple routes) of C=N double bonds over C_2H_4O@NH_2-Cu_1/Pd(111). (c) The reaction of H with the N atoms (black routes) and C atoms (purple routes) of C=N double bonds over C_3H_6O@NH_2-Cu_1/Pd(111). (d) The free energy profiles for H reactions with C=N and C=C double bonds over C_3H_4O@NH_2-Cu_1/Pd(111). The green, black, purple, and blue routes represented that the H reacted with N, C, C_1, and C_2 atoms, respectively. TS represented the transition state. The cyan, grey, white, blue, and yellow spheres represented Pd, C, H, N, and Cu atoms, respectively.

Table S10 The free energy barriers (eV) for H reactions with functional groups and CO_2 over structures. RDS represented the rate-determining step for CO_2 hydrogenation to CH_3OH on various structures.

Structures	NH_2	C=N double bond		C=C double bond		RDS
		C	N	C_1	C_2	
NH_2-Cu_1/Pd(111)	1.07	—	—	—	—	0.88
C_2H_4O@NH_2-Cu_1/Pd(111)	—	1.05	1.41	—	—	0.79
C_3H_4O@NH_2-Cu_1/Pd(111)	—	1.28	0.95	0.85	0.77	0.66
C_3H_6O@NH_2-Cu_1/Pd(111)	—	1.38	1.59	—	—	0.86

The effect of support on catalytic performance

Supports can affect the activity, selectivity, and yield of products by regulating the active site, adsorption strength, coordination environment, binding energy and the chemical state of metal species, etc.[S12-S14] For example, Bai et al. investigated the influence of supports (SiO_2, CeO_2, Al_2O_3 and P_{25}) on the catalytic performance of Pd_2Cu NPs. They found that Pd_2Cu NPs/CeO_2 showed the highest CH_3OH yield due to CeO_2 enhancing the activity of Cu. Pd_2Cu NPs/P_{25} had the highest selectivity for C_2H_5OH owing to oxygen vacancies on P_{25}.[S15] In addition, Jiang et al. reported that the formation rate of CH_3OH over supported Pd-Cu catalysts decreased in the following order: amorphous silica > SBA-15 > MCM-41 > MSU-F. Among the four supports, the amorphous silica supported Pd-Cu catalysts exhibited the highest selectivity for CH_3OH.[S16]

Furthermore, we used DFT calculations to explore the effect of support on CO_2 adsorption in the revised manuscript. During the study, SiO_2 was chosen as the support for Pd-Cu nanoparticles (PdCu NPs/SiO_2) to determine the adsorption energy of CO_2. As shown in Fig.S16†, the adsorption energy of CO_2 on PdCu NPs/SiO_2 was -0.97 eV, which was stronger than that on Cu_1/Pd(111) (-0.12 eV). The result indicated that the support had a significant effect on CO_2 adsorption through tuning the electronic structure, which was consistent with previous studies.[S17]

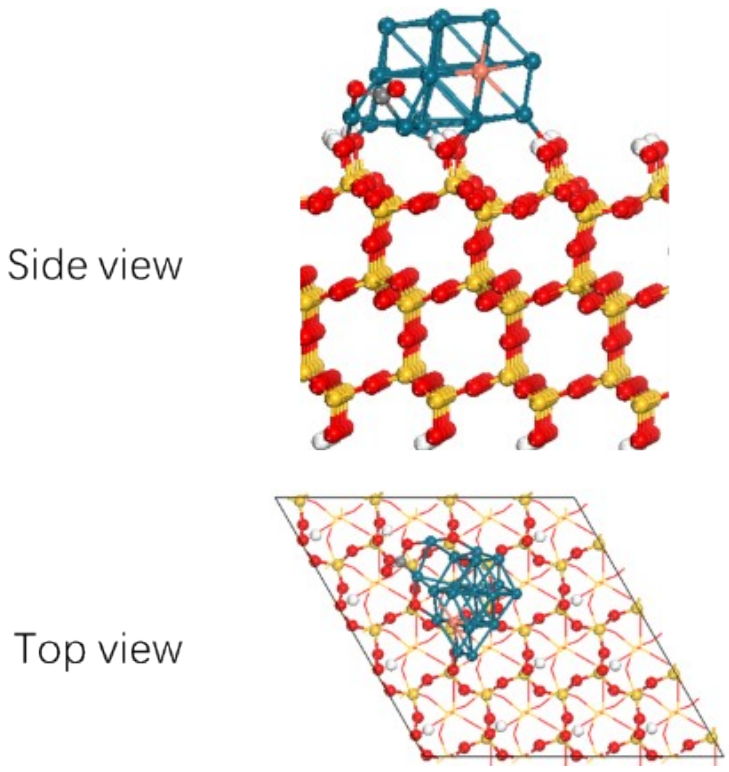

Fig. S16 The adsorption of CO_2 on PdCu NPs/SiO_2. The cyan, grey, white, red, orange, and yellow spheres represented Pd, C, H, O, Si and Cu atoms, respectively.

References

S1 C. Stegelmann, A. Andreasen, C. T. Campbell, *J. Am. Chem. Soc.*, 2009, **131**, 8077-8082.

S2 C. T. Campbell, *ACS Catal.,* 2017, **7**, 2770-2779.

S3 S. Kozuch, S. Shaik, *J. Phys. Chem. A*, 2008, **112**, 6032-6041.

S4 S. Kattel, P.J. Ramírez, J.G. Chen, J.A. Rodriguez, P. Liu, *Science*, 2017, **355**, 1296-1299.

S5 Q. Tang, Z. Shen, C.K. Russell, M. Fan, *J. Phys. Chem. C*, 2018, **122**, 315-330.

S6 S. Kattel, B. Yan, Y. Yang, J.G. Chen, P. Liu, *J. Am. Chem. Soc.*, 2016, **138**, 12440-12450.

S7 Y. Peng, L. Wang, Q. Luo, Y. Cao, Y. Dai, Z. Li, H. Li, X. Zheng, W. Yan, J. Yang, J. Zeng, *Chem*, 2018, **4**, 613-625.

S8 J. Ye, C. Liu, D. Mei, Q. Ge, *ACS Catal.*, 2013, **3**, 1296-1306.

S9 J. Liu, Q. Ke, X. Chen, *J. Mater. Sci.*, 2021, **56**, 3790-3803.

S10 L. Liu, H. Yao, Z. Jiang, T. Fang, *Appl. Surf. Sci.*, 2018, **451**, 333-345.

S11 L. Liu, F. Fan, Z. Jiang, X. Gao, J. Wei, T. Fang, *J. Phys. Chem. C,* 2017, **121**, 26287-26299.

S12 S. Li, X. Yao, Y. Chen, *Angew. Chem. Int. Ed*, 2017, **56**, 10761-10765.

S13 Z. Li, R. Wu, L. Zhao, X. X. Wei, J. J. Wang, J. S. Chen, T. R. Zhang, *Nano Res.,* 2021, **14**, 3795-3809.

S14 J. Y. Park, L. R. Baker, G. A. Somorjai, *Chem. Rev.*, 2015, **115**, 2781-2817.

S15 S. X. Bai, Q. Shao, P. T. Wang, Q. G. Dai, X. Y. Wang, X. Q. Huang, *J. Am. Chem. Soc.*, 2017, **139**, 20, 6827-6830

S16 X. Jiang, N. Koizumi, X. Guo, *Appl. Catal. B: Environ.,* 2015, **170**, 173-185.

S17 F. Lin, X. Jiang, N. Boreriboon, Z. H. Wang, C. S. Song, K. F. Cen, *Appl. Catal. A: Gen.,* 2019, **585**, 117210.